frontiers | Frontiers in Analytical Science

TYPE Original Research
PUBLISHED 18 December 2024
DOI 10.3389/frans.2024.1518243

OPEN ACCESS

EDITED BY
Ying Liu,
Nanjing University, China

REVIEWED BY
Changyu Wu,
Xuzhou Medical University, China
Zhanjun Yang,
Yangzhou University, China

*CORRESPONDENCE
Quan Cheng,
quan.cheng@ucr.edu

RECEIVED 28 October 2024
ACCEPTED 03 December 2024
PUBLISHED 18 December 2024

CITATION
Rais NA, Abouhajar F, Stuart DD, Van Zant W and Cheng Q (2024) Surface plasmon resonance to trace and measure cancer cell apoptosis using morphological and refractive index changes. *Front. Anal. Sci.* 4:1518243.
doi: 10.3389/frans.2024.1518243

Surface plasmon resonance to trace and measure cancer cell apoptosis using morphological and refractive index changes

Nor Akmaliza Rais, Fatimah Abouhajar, Daniel D. Stuart, Westley Van Zant and Quan Cheng*

Department of Chemistry, University of California, Riverside, Riverside, CA, United States

Morphological changes of cancer cells are often used as an important indicator within efficiency studies of anticancer drugs. Morphological cell analysis on cell size and shape distribution is typically performed using microscopic methods, which are time consuming and require skilled personnel. Recently, more advanced image processing and pattern recognition have enabled identification and quantitative analysis of the cell's abnormality and classification in an automated way. However, these methods usually involve multiple staining steps. In addition to computational complexity, the processes greatly compromise real-time applications of the system. Therefore, a non-invasive, real-time method allowing for assessment of living cells' reactions to a death inducer is very much needed. Here, we present an SPR biosensor that measures the changes in cancer cells' size and detachment, relating the cell confluency with the changes of the refractive index on the cell-substrate interface. As a proof-of-concept, we chose HeLa cell and hydrogen peroxide (H_2O_2) induced apoptosis as the model system to study the morphological changes of the cell. The results show that the SPR response to cell apoptosis agreed with the cellular morphological changes observed via microscopy. Interestingly, we observed simultaneous apoptosis and necrosis at high H_2O_2 concentrations. This simultaneous occurrence was verified using a mathematical model which incorporated other important factors such as cell thickness and intercellular refractive index. This model helped resolve the disagreement between SPR signal and cell confluency at high H_2O_2 concentrations. Our results show the potential of SPR as a label free and real time monitoring method for morphological changes and surface detachment of cancer cells. This method can be fully expanded to other cell-based sensing applications.

KEYWORDS

cell morphology, surface plasmon resonance, apoptosis, necrosis, cell-based sensing

Introduction

Cancer remains one of the biggest human health challenges we face today. For example, a total of 570,000 cases and 311, 000 deaths were estimated for cervical cancer in 2018, making this disease the fourth most frequently diagnosed and leading cause of cancer death in women (Bray et al., 2018). Current treatments for cervical cancer include surgery, radiation and chemotherapy. Follow-ups after treatment are also required to check for recurrences and to screen for possible complications (Author Anonymous, 2019). Most clinical trials for patients with cervical cancer involve development of drugs that induce

apoptosis, a type of cell death (Lowe and Lin, 2000). Thus, recent advances in cervical cancer studies have mainly focused on identifying agents that can selectively induce cytotoxicity and stimulate the apoptosis caused by anticancer agents.

Cell apoptosis involves a large variety of events for which several robust molecular markers exist. Among the most widely used cell-based assays include MTT assay (Gomez Perez et al., 2017), TUNEL assay (Kateryna et al., 2012), and LDH Cytotoxicity assay (Smith et al., 2011), which measure cell metabolism, DNA fragmentation and cell cytotoxicity, respectively. Semi-quantitative label-free assays also exist and usually involve microscopic identification of change in morphological features occurring during the apoptotic process (e.g., cell rounding, membrane blebbing as well as the condensation and fragmentation of the nucleus content) (Elmore, 2007). Although morphological assays are label free, they are limited in resolution and are therefore unable to observe changes on the cell-substrate interface of adhered cells without being destructive to the cells. Therefore, there is a need for cell-based nondestructive and label-free technology that allows for quantification of morphological changes associated with apoptotic processes.

Promising candidates of such technologies are surface sensitive methods, such as surface plasmon resonance (SPR). Cell-based SPR sensors are desirable due to the real-time label free analysis they provide and their ability to monitor protein interactions like those involved in the cell-substrate interface that is notoriously difficult to visualize with microscopic techniques. As such, SPR as a surface-sensitive method is usually used for studies and quantifying cell-substrate interactions of adhered cells. For example, SPR can quantify responses to cell sedimentation, deposition and spreading processes as well as cell attachment area as the result of the cells' responses to biological and chemical stimuli (Deng et al., 2016; Maltais et al., 2012; Yanase et al., 2007). However, the actual mechanism of how the physical alterations of the cells affect SPR signal still remains elusive as there is limited literature on SPR detection of whole cells. One study relates the change of density on the sensor chip to the increase in SPR signal after the stimulation (Chen et al., 2010). SPR was also used to study morphological changes of cells in response to stimulation agents and cell death inducers (Maltais et al., 2012; Yanase et al., 2007; Chen et al., 2010; Chabot et al., 2009).

More recent cell-based SPR studies have begun to consider the influence of the cell's own refractive index on observed SPR responses. A study showed that intercellular cell components such as the membrane and nucleus possess a different refractive index, which can contribute to SPR signals (Minet et al., 1996). It was also found that cellular refractive index is distributed throughout the cell body and values vary at different stages of cell death (Zhang et al., 2017). The influence of refractive index in cell bodies to SPR signal was demonstrated in a study which found that the SPR signal increases as the volume of the cell decreases due to cytoplasmic concentration increases causing an increase in the cellular refractive index (Robelek and Wegener, 2010). The same conclusion was made by a study of exocytosis of cells, where a shift of the resonance angle was observed due to an elevated concentration of secretory vesicles close to the cell membrane (Moreira et al., 2017).

In this study, we systematically investigated the SPR response to cell size, deformity and detachment, by relating SPR signal to the percentage of the surface of a substrate that is covered by adherent cells, known as cell confluency. As a proof-of-concept, we chose HeLa cells and hydrogen peroxide (H_2O_2) induced apoptosis as the model system. Hydrogen peroxide, as a reactive oxygen species (ROS), induces apoptosis in HeLa cells through the intrinsic mitochondrial pathway by several proposed mechanisms. Studies have suggested that apoptosis induced by H_2O_2 is mediated by decreased superoxide (O^{2-}) concentration (Marie-Veèronique et al., 1998) and by activation of p73 pro-apoptotic genes, which trigger apoptosis in response to DNA damaging agents (Singh et al., 2007).

The ability of SPR to detect and quantify morphological characteristics of cells is particularly useful for diagnosing cancer and in studying the efficacy of anticancer drugs. For the diagnosis, cancer cells can be detected and classified by specific features including their shape and size, as well as the distribution of the cells (Kumar et al., 2015). This is useful when comparing normal, pre-cancer and malignant cells, as demonstrated in studies of breast cancer (Rajbongshi et al., 2018; Hemminki and Granström, 2002) and cervical cancer. (Rahmadwati et al., 2012). Moreover, SPR does not require the cells to be fixed to preserve the cells, which is commonly required in other microscopic methods. However, the physical features more related to SPR capability are the cell-cell and cell-substrate interactions. For example, cancer cells often become disordered and less adherent to the other cells and to the extracellular matrix (Cooper, 2000), which cause the changes in confluency and optical properties on the interface. Both traits are measurable by SPR.

In this work, the change of SPR response towards HeLa cell morphological changes on the sensor chips was studied. Experimentally, HeLa cells were cultured on SPR chips until 80%–100% confluent monolayer was achieved. SPR measurements were then carried out with different concentrations of H_2O_2. Another set of chips were prepared in a six-well culture plate for a microscopic experiment that replicated the SPR experiment. Then, the SPR sensorgram results compared with cell confluency data after the images were processed with Fiji/ImageJ (Schindelin et al., 2012). In addition, a mathematical model based on SPR refractive index changes was employed to explain the underlying refractive index shifts that are associated with confluency changes.

Experimental section

Materials and solutions

The human cervical cancer HeLa cell line was purchased from American Type Culture Collection (ATCC) and cryopreserved in liquid nitrogen storage until use. Dulbecco's Modified Eagle Medium (DMEM), Fetal bovine serum (FBS), Penicillin, Streptomycin, 0.05% Trypsin-EDTA from Gibco. Hydrogen peroxide (H_2O_2) was purchased from Sigma-Aldrich. Buffered salt solution (HBSS) which contains 10 mM HEPES, 150 mM NaCl, 5 mM KCl, 1.2 mM $MgCl_2$, 2 mM $CaCl_2$ and 10 mM D-glucose, pH 7.4 adjusted with NaOH. The buffer was filtered, degassed and autoclaved before use.

Apparatus

For cell culture, a Class II A/B3 biological safety cabinet, Fisher Scientific ISOTEMP 205 water bath, Pelton & Crane Validator

8 autoclave, CF-80-1 electronic centrifuge, Fisher Scientific CO_2 incubator and Kenmore lab refrigerator were used. Microscopic imaging was done with an Omano microscope with an AmScope digital camera. The refractive index of various liquid solutions was measured with American Optical ABBE refractometer. SPR data was measured with NanoSPR 3 (Addison, IL) with 650 nm GaAs semiconductor laser light source and Orion Sage syringe pump. Nanopure water (>18 MΩ), purified through a Barnstead E-Pure filtration system (Thermo Scientific, Rockford, IL) was used for all reagent preparations and rinsing.

Culturing of HeLa cells

HeLa cells were cultured in DMEM supplemented with 10% FBS and 1% penicillin and streptomycin. Cells were incubated at 37°C and 5% CO_2 in a humidified incubator. The culture medium was removed from the culture flask. Then, cells were detached by a standard trypsinization protocol. For this purpose, 2 mL of 0.05% trypsin-EDTA was added into the culture flask and placed in the incubator to allow the trypsin to work. The flask was observed under the microscope every minute until the cell was slightly detached from the flask wall and appeared rounded and separated from each other. Thereafter, the Trypsin-EDTA solution was aspirated out prior to adding a 5 mL of fresh medium to resuspend the cells. Then, the cells were gently pipetted several times to ensure that the cells are transferred and dispersed into the fresh medium. After that, 2 mL of the cell suspension was transferred into a new culture flask and resuspended in 5 mL of fresh medium. The cells were kept in an incubator and subcultures of confluent cells were performed every 1–2 days.

Culturing of HeLa cells on SPR chips

Gold chips from glass slides were fabricated via layer by layer deposition of 4 nm Chromium and 50 nm gold, using an electron beam physical vapor deposition system within the cleanroom facility at UCR as has been discussed in previously published procedures (Hinman et al., 2015). Prior to use, the chips were rinsed with Nanopure water, ethanol, air dried and then sterilized via UV radiation overnight. Following this clean gold chips (2.5 × 1.5 cm) were placed in each well of a 6-well cell culture plate. For cell suspension preparation, HeLa cells were removed from culture flasks by trypsinization, suspended in 8 mL of culture medium. An aliquot of 1 mL suspension and 3 mL of culture medium were pipetted on top of the SPR chip into each well. Each well's content was inspected via microscopy for uniform distribution of cells. The plate containing the SPR chips was then kept in the incubator for 1–2 days until their surfaces were covered with ~80–100% layer of cells, prior to use for SPR experiments.

SPR measurements

The measurements of SPR signal response to HeLa cells death were performed on a dual channel SPR spectrometer (NanoSPR-3) equipped with a Plasmon Serial software, which provides real-time reflectivity curves and sensorgrams of the real-time minimum angle. All SPR measurements were conducted at room temperature (22.5°C) with syringe pump flow set to 5.0 mL/hr. As such, HBSS was employed as the running buffer as this buffer is recommended to keep cells viable for a longer period of time at room temperature without CO_2 supply (Moreira et al., 2017). Buffer flow rate across the sensor surface was precisely controlled using a syringe pump which also could be set on pause mode for incubation purposes. Prior to measurements, the chambers, inlet/outlet tubing, injection ports and all device accessories were sterilized with 70% (v/v) ethanol for 30 min and then rinsed with HBSS.

Once the cells had reached confluency on the SPR chip, the back side of the chips were cleaned with 70% ethanol and water. Then, the chip was adhered to the prism using a refractive index matching fluid (n = 1.571 Cargille Laboratories New Jersey). The flow cell, consisting of two 30 μL flow channels, was attached afterwards, and the buffer flows were run for 30 min to obtain a stable baseline. Next, different concentrations of H_2O_2 were introduced into the sensing chamber and the flow was stopped. The signal was monitored until no further changes in resonant angle were observed for at least 40 min before the flow pump was turned on for rinsing. After measurements were completed, the outlet was disposed of in a hazardous biological waste container and instrument parts were again cleaned with 70% ethanol.

Microscope examination of the cell covered SPR chips after treatment with different concentration of H_2O_2

All chips were examined for cell viability and confluency using microscopy prior to investigating H_2O_2-HeLa cell interactions, which were monitored by both SPR and microscopic imaging. For relating SPR response to cell confluency, the microscope imaging was performed at conditions replicating the SPR experiments. The chips were removed from the incubator and were placed in a 6-well plate staged on the microscope platform. 5 mL of HBSS buffer was added into the wells which was left to incubate for 30 min. The cell images were taken at several time intervals using the digital microscope camera before and after exposure to H_2O_2 at 25x magnification. To ensure accuracy, the images were taken at the same spot on the chips.

Cell confluency measurement

Prior to imaging, a calibration was performed using a stage micrometer to ensure accurate size measurements. The cell coverage on the chip was calculated via Fiji/Image-J software (Schindelin et al., 2012). To quantify the fraction of covered areas, cell boundaries were traced manually using the freehand selection tool. Then, the cell interior was filled by means of a fill-hole procedure. In this way, the cell covered area was distinguished from the cell-free area via a threshold function. The particle analysis tool was used to calculate the percentage of covered area, which was also use to determine cell confluency. This method provided cell number, cell density and cell shapes, which are

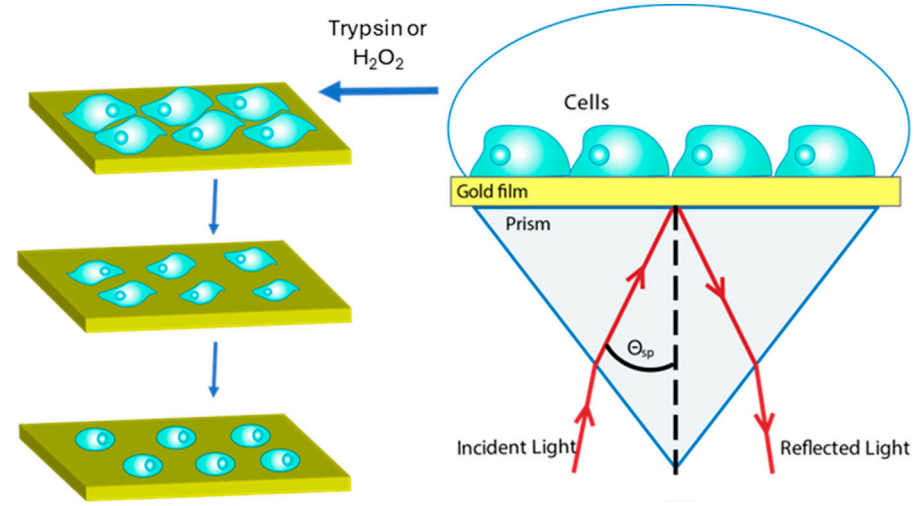

FIGURE 1
Experimental setup. SPR monitors cell morphology changes induced by chemical treatment in real time without any labeling requirements. Morphological changes of surface-adhered cells induce refractive index changes within that region, which can be tracked via SPR.

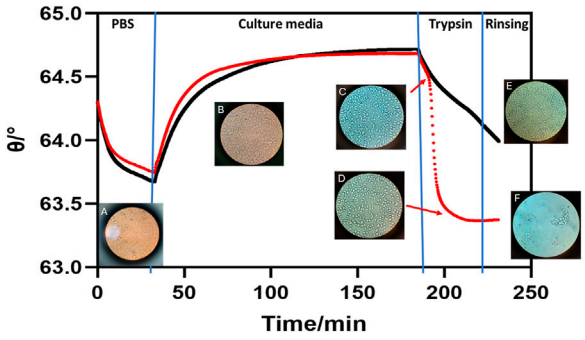

FIGURE 2
SPR sensorgram showing HeLa cell detachment progress mediated by trypsin (red line) and PBS control (black line). Microscopy images are overlayed at their respective time points within the sensorgram. **(A)** HeLa cells on the sensor chip in PBS at the start of the experiment. **(B)** Cells incubated in culture media (HBSS) showing robust confluency. **(C)** HeLa cells at the start of incubation with 0.05% trypsin already showing shrinkage which matches with a drop in SPR signal. **(D)** Cells dissociating from the surface during the trypsin treatment resulting in a rapid decrease in SPR signal. **(E)** Cells in the control channel remaining on the sensor surface after a PBS injection and rinse. **(F)** Image of the sensor surface following trypsin treatment where detached cells are clearly rinsed off.

useful in cell-based assays and in the estimation of adherent cell culture characteristics.

Result and discussion

Characterization of the SPR system for monitoring living cells

Trypsin is a pancreatic serine protease with substrate specificity towards positively charged lysine and arginine side chains (Brown and Wold, 1973). Due to this, trypsin is widely used to detach adherent cells from the surface of culture flasks through its ability to orderly and unambiguously cleave cellular adhesion proteins. As such, trypsin appears as an ideal first step to confirm that our SPR system can be applied to monitoring cell-surface interactions through the disruption of these interactions. A scheme of the SPR cell morphology experimental setup and sensing system is shown in Figure 1.

In the initial study, 10 mM PBS (137 mM NaCl, 2.7 mM KCl, 10 mM Na_2HPO_4 and 1.8 mM KH_2PO_4) was used as the running buffer. After a 30 min buffer baseline, HeLa cells were incubated with culture medium for 2.5 h before rinsing for 5 min. Next, (0.05%) trypsin solution was injected into the flow cell and incubated for 20 min followed by running buffer for rinsing. For comparison purposes, time-lapse microscopic images were also captured on a separate setup that is in line with the timing of the SPR experiment.

As shown in Figure 2, the SPR signal decreased rapidly after 4 min of incubation with trypsin. At the same time, the microscopic image shows a confluency decrease as surface-adhered area decreases, cells become smaller, and more rounded (images inserted in Figure 2). As the trypsinization continued the SPR signal continued to decrease at a fast rate, with an overall change of 1.0° ($\Delta\Theta$ = 1.0°) observed, before plateauing once the cells completely detached from the surface during the rinsing step (Figure 2).

To further confirm that the SPR signal decreases as a result of cell detachment and not by other factors such as temperature, replacement of cell growth media, or buffer flow shear, a control was conducted with an injection of PBS buffer instead of trypsin. As shown in Figure 2 the rate of signal decrease was substantially smaller than that of the trypsin-treated channel. In addition, the cells maintain their shape even after the rinsing, as shown by the microscopic image (Figure 2; Supplementary Figure S1). This confirmed that cell morphological changes induced by cell detachment could be easily differentiated from the removal of

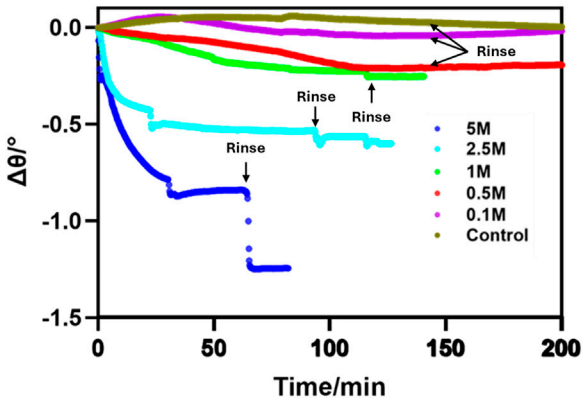

FIGURE 3
SPR sensorgram showing SPR signal change as a function of time when HeLa cells are treated with different concentrations of H_2O_2. The sensorgrams begin with injection of H_2O_2 as time point zero.

culture medium. This result demonstrates that our SPR system is sensitive to changes in cell confluency and attachment. The observed trends agree with other results in literature, where it was also demonstrated that the effective refractive index decreases as cells detach from the surface (Deng et al., 2016; Moreira et al., 2017).

SPR monitoring of cell morphological changes after exposure to H_2O_2

Cell morphological change, and specifically the reduced size due to shrinkage, is a distinguishing feature of HeLa cell death induced by apoptosis. Therefore, cell confluency measurements could be used to evaluate the relationship between SPR response and HeLa cell toxicity. After a 50-minute baseline, 1 M of H_2O_2 was injected into the experiment channel while HBSS was injected into the control channel. Then, the change in SPR response was monitored for 120 min before flowing the buffer for rinsing. Supplementary Figure S2 shows the SPR signal response of a HeLa cell to 1 M of H_2O_2. After H_2O_2 injection, the SPR signal decreases ($\Delta\Theta$ = 0.3°) while the control channel remains steady.

Next, the experiment was repeated for different concentrations of H_2O_2, with results summarized in Figure 3, which exhibited a concentration dependent response. The lowest concentration (0.1 M) had little effect on HeLa cell apoptosis as the SPR signal is nearly unchanged. However, higher hydrogen peroxide concentrations are associated with negative SPR signal shifts. The calculated resonance angle decreases of different concentrations of H_2O_2 are as follows: 0.2, 0.3, 0.5 and 0.9-degree shifts ($\Delta\Theta$) for 0.5, 1.0, 2.5 and 5.0 M, respectively.

Interestingly, after treating HeLa cells with a higher concentration (5 M) of H_2O_2, the SPR signal decreased at a rapid rate and achieving a steady signal after 25 min (Figure 3). During the rinsing step (after a 60-min incubation), the signal showed a drastic drop as all cells were detached from the surface. A similar but muted effect was seen with the lower concentrations of H_2O_2 as a much smaller proportion of the cells were detached by the treatment and subsequent rinse. These results confirm that the highest concentration of H_2O_2 (5 M) led to the strongest toxicity effect to HeLa cells, indicating that the system is sensitive to concentration dependent differences in morphological changes.

Microscopy images of cell morphology changes after exposure to H_2O_2

To quantify the cell confluency and compare with our SPR signal, microscopy time-lapse images were collected for 0.1, 0.5, 1.0, 2.5 and 5.0 M of H_2O_2. The images show a decrease in cell size and an increase in the amount of intercellular space, due to apoptosis. To calculate the attachment area, images were processed with Fiji/ImageJ software. The resulting images of HeLa cells after treatment with 1.0 M H_2O_2 can be seen in Supplementary Figure S3. The confluency extracted from these images are as follows: 85%, 60%, 50%, 45% and 40%, at 0, 30, 60, 90 min and 120 min, respectively. Confluency decreased over the incubation time as H_2O_2's reactive oxygen species lead to apoptosis. However, with 5.0 M H_2O_2 as shown in Figure 4 the measured confluency (90%, 43%, 34%, 43%, and 37%) dropped much faster but then had a brief increase before continuing its downward trend. This may be attributable to necrosis occurring in addition to apoptosis that would induce a separate and different morphological change, the combination of which may not be directly related to confluency.

Necrosis is characterized as the degradative processes that occur after cell death and does not follow the apoptotic signal transduction pathway (Elmore, 2007). Usually, apoptosis progresses to necrosis but both can also occur simultaneously depending on factors such as the intensity and duration of the stimulus (Zeiss, 2003). As the 5.0 M H_2O_2 causes rapid apoptosis it is likely that apoptosis and necrosis are occurring simultaneously. Necrosis is distinguished from apoptosis by the difference in morphological changes as observed by cell swelling, loss of membrane integrity and possible release of the cytoplasmic contents into the surrounding area (Zeiss, 2003; Joris and Joris, 1995).

Observing the images in Figure 4C in more detail indicates that in the first 2 min of exposure to 5.0 M H_2O_2 HeLa cells undergo apoptosis, as exhibited by cell rounding and shrinkage. Within 4 min, some cells started to disintegrate, and the cell inner body began to rupture, indicating early necrosis, while other cells remained apoptotic. After 6 min, cell swelling was observed and the number of necrotic cells increased. This observation was in agreement with results reported in a study that distinguished cell death induced by apoptotic and necrotic treatment of HeLa cells (Rello et al., 2005). In the study, necrotic cells were characterized by loss of control of the water influx through the plasma membrane and then loss of membrane integrity, as well as liberation of cytoplasmic content during early necrosis, followed by uniform condensation and fragmentation of the chromatin. In the late stage of necrosis, cell flattening occurred, and eventually the cell body completely detached while some debris remained on the surface. The cell detachment of the cell bodies at the end of necrosis could be the reason for the decreased confluency after 30 min. Even though we were able to validate the trend in cell confluency induced by 5.0 M H_2O_2, the reason why SPR does not respond with the same trend remained unexplained. Clearly, the combination of different morphological features of apoptosis and necrosis are affecting SPR response, which provoked us to reexamine the biophysical

10.3389/frans.2024.1518243

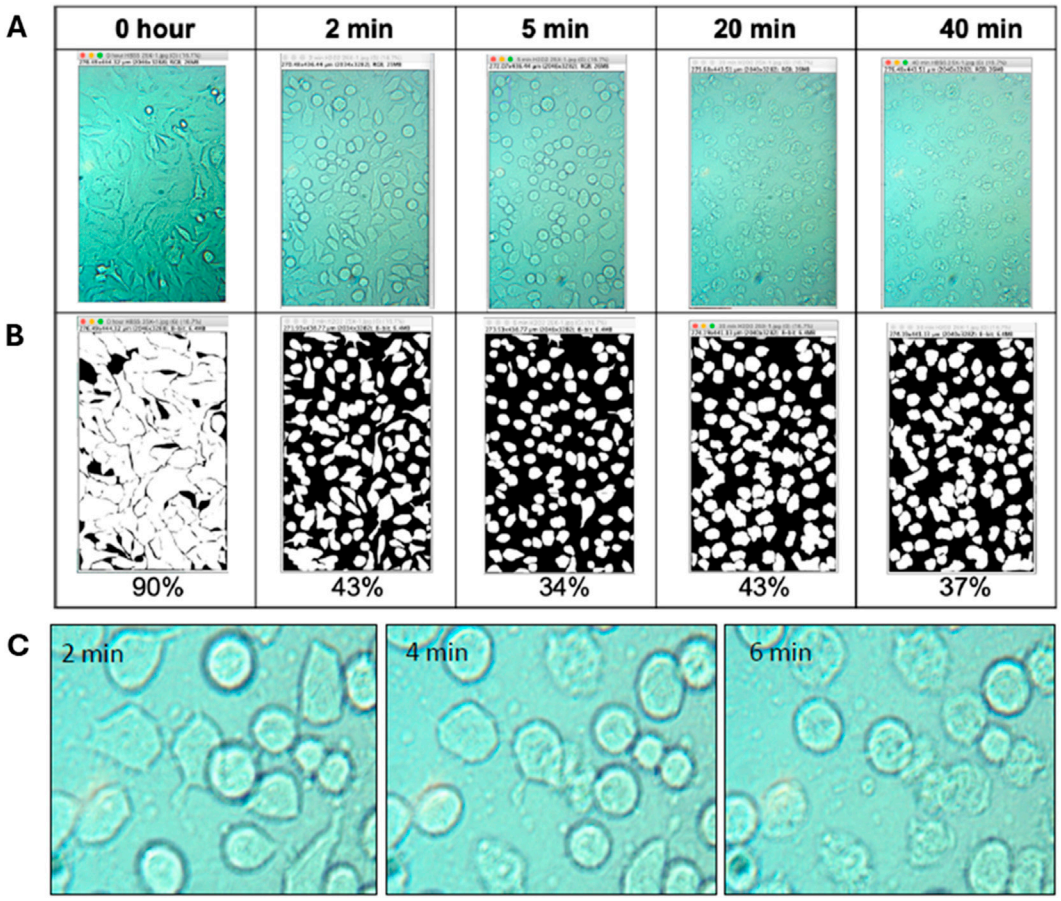

FIGURE 4
Images of HeLa cells exposed to 5.0 M H_2O_2 over time. **(A)** Shows the original images and **(B)** shows ImageJ threshold processed images with their respective percentage confluency. **(C)** Time based images of HeLa cells apoptotic and necrotic features induced by 5.0 M H_2O_2.

changes of the cell-substrate interface, as these contribute more toward changes of SPR signal than the cell morphology.

Mathematical modeling and comparison between calculated and measured SPR signal

SPR response to a single layer of uniform thickness

A mathematical relationship between the SPR signal and the adsorbed film thickness and coverage was previously established based on the effective refractive index model (Linda et al., 1998). This model allows quantitative analysis to predict the response of an SPR sensor when a molecule or adsorbate (for example, thiolate, protein and cell monolayer) binds on an SPR surface and the adsorbate has a different refractive index from the bulk solution. The theoretical description for the SPR signal response to a uniform layer of adsorbate is shown in Figure 5.

For such structures, a thin film of uniform thickness d and refractive index of ηa is adsorbed to the metal surface of SPR chip, while a bulk liquid solution with refractive index ηs is above the layer, and the SPR response in angle shift (ΔΘ) can be calculated using Equation 1.

$$R = m(\eta_a - \eta_s)\left[1 - e^{\frac{-2d}{l_d}}\right] \quad (1)$$

where R is the SPR response as the shift in angle (ΔΘ), m is the slope of the calibration curve, which is also the sensitivity factor for SPR, η_s and η_a is the refractive index for the bulk solution and the film layer, d is the thickness of film and ld is the characteristic decay length, which is 20%–50% of the wavelength of light source used in SPR.

This equation was simplified from the estimation that the effective refractive index of the bilayer, η_{eff}, is the properly weighted average of ηa plus ηs. Other assumptions made in this model are that the evanescent electromagnetic field decays exponentially into this medium with a characteristic decay length, ld, ~25–50% of the wavelength of the incident light, and the intensity of light is the field strength squared, so it decays with height z above the metal surface as $e^{-z/ld}$ (Yanase et al., 2014). The above assumption is valid for an SPR response that is linearly proportional to the change of refractive index over the range η_a + η_s.

NaCl solutions exhibit great linearity of RI *versus* concentration and thus can be used as the RI fluid for experiment to determine SPR sensitivity and dynamic range. Therefore, 0.5, 1.0, 1.5, 2.5, 3.0 and 5.0 M NaCl solutions were injected in sequence and each injection

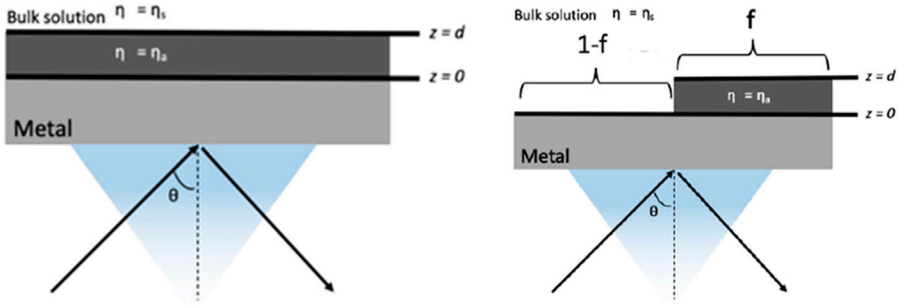

FIGURE 5
Schematic diagrams of the working interface of a thin metal film in contact with a bilayer structure consisting of (right) a uniform layer adsorbate (left) a nonuniform coverage and bulk solution *s*. Based on equations from ref (Linda et al., 1998)

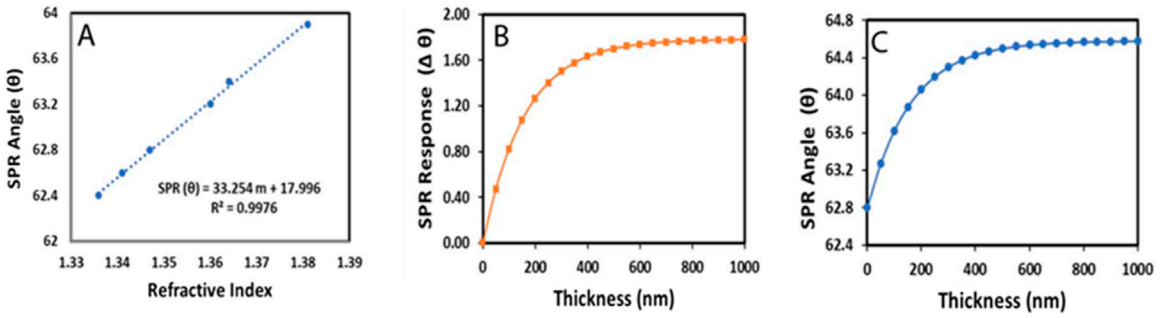

FIGURE 6
The fitted curve of SPR response *versus* the refractive index of bulk NaCl solution **(A)** Calculated SPR response *versus* thickness *d*, in angle shift **(B)** and in angle **(C)**, for HeLa cells monolayer on a gold chip in HBSS solution, as represented on Figure 5.

TABLE 1 Comparison of experimental and calculated SPR angle shift for different buffers.

Bulk solution	RI	$\theta_{calculated}$	$\theta_{experimental}$
DIW	1.334	62.4°	62.3°
PBS	1.338	62.5°	62.6°
HBSS	1.338	62.5°	62.8°
5.0 M H_2O_2	1.345	62.7°	63.0°

was separated by a buffer wash. The fitted curve (Figure 6A) shows the dynamic range of the SPR system is from 1.336 to 1.381. The accuracy and stability of our SPR measurements were verified by comparing the SPR angle measured for different buffers with the calculated values from the equation obtained from the calibration curve. The data were compiled in Table 1, showing good agreement between SPR angles obtained from experimental and calculated data, for different types of buffer solutions.

To predict the response of SPR sensor with a HeLa cell adsorbed on a gold chip, first we calculate the SPR response in ΔΘ as a function of adlayer thickness as predicted in Equation 1, using a HeLa cell refractive index (η_a) of 1.39 (Deng et al., 2016), a Buffer refractive index (η_a) of 1.338, an SPR sensitivity factor of 33, a characteristic decay length (l_d) of 325 nm (50% of λ), and an adsorbate layer thickness (d) from 0 to 1,000 (nm). The predicted SPR response is shown in Figure 6B. Then, we plot the curve in SPR angle Θ, taking 62.8° as the initial angle when there is no cell layer on the surface (Figure 6C). From these plots, we can estimate the thickness of the cell layer from the measured and calculated SPR response. Based on our data, the measurable thickness of HeLa cells is less than 300 nm. In addition, we can see that after 400 nm, the SPR response is no longer sensitive to changes in the cell-substrate interface. However, after Hela cell treatment with H_2O_2, the cell undergoes morphological change during the apoptosis process and cover the gold surface nonuniformly. Therefore, inclusion of nonuniform coverage is needed to calculate the SPR response after HeLa cell treatment with the stimuli.

SPR response to a nonuniform coverage adsorbate

The structure in Figure 5 on left as previously reported considers nonuniform adsorbate coverage, where the adsorbate covers a fraction (*f*) of the metal surface with thickness of *d*. In this case, the SPR response is just *f* times the response when $f = 1$, which is the SPR response for uniform coverage calculated using Equation 2. We then used the correlation to calculate the SPR response as a function of percentage of cell confluency (*f*) as in Equation 2.

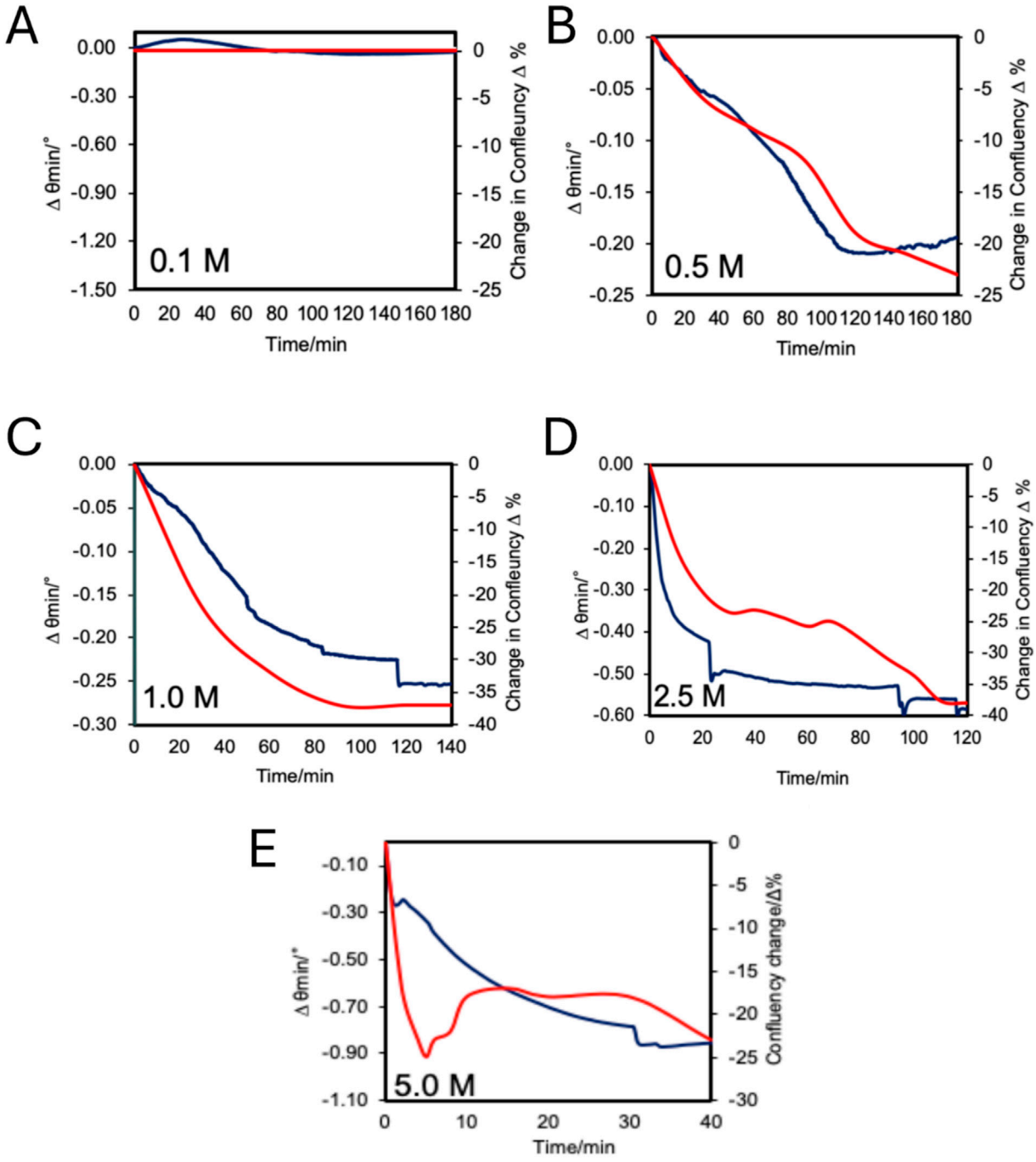

FIGURE 7
Changes in SPR minimum reflectivity angle (Blue) and cell confluency (Red) measured over time during H_2O_2 treatments **(A)** 0.1 M, **(B)** 0.5 M, **(C)** 1.0 M, **(D)** 2.5 M, and **(E)** 5.0 M.

$$R_{non-uniform} = f \, x \, R_{uniform} \quad (2)$$

This assumption is valid when the thickness, *d*, is less than or equal to *l*d, which is true in our case. For a very small thickness, the response of a nonuniform structure would be the same as that of a uniform structure, while for a very large thickness it would give a complex SPR with a double minimum reflectivity curve, where any material further away from the metal surface does not contribute strongly to the SPR response.

Comparison between measured and calculated SPR response to cell confluency

The thickness of the uniform cell layer was determined from the SPR angle at baseline before H_2O_2 was injected and by using the angle-thickness data in Figure 6C. After the thickness was obtained,

we were able to calculate ΔΘ when $f = 1$, which is the SPR response calculated by Equation 1 at each concentration of H_2O_2 where the refractive index of the HeLa cell (ηa) = 1.339, the refractive index of the H_2O_2 solution (ηs) used were as follows: 1.3365, 1.3377, 1.3389, 1.3419, and 1.3476 for 0.1, 0.5, 1.0, 2.5 and 5.0 M, respectively. Therefore, the data of $R_{nonuniform}$ were calculated by Equation 2 which is equal to the calculated $R_{uniform}$ times the percentage of confluency.

Figure 7 illustrates a comparison between measured and calculated SPR response extracted from Equation 2 according to HeLa cell confluency change after its treatment with different concentrations of H_2O_2. The correlations between SPR angular and confluency changes are better at lower concentrations of H_2O_2. However, at a higher concentration (5 M) abnormal behavior of the SPR response was observed. The calculated response does not follow the experimental data after 5 min of exposure, where the signal increases instead of continuing to decrease.

Relationship between SPR signal and cell confluency

To evaluate the correlation between SPR response data and the cell confluency change data during the apoptosis process under hydrogen peroxide treatment, both sets of data for each H_2O_2 concentration were plotted on the same graph (Figure 7). The results show that, in general, the SPR response agrees with confluency change measured by microscopy experiments. When observing the slope of each curve in Figure 7, it shows a higher rate of change at the beginning of the measurements for all H_2O_2 concentrations, with exception of the 0.1 M concentration. The shape of the curves for the SPR response and cell confluency closely match at lower concentrations (0.1, 0.5, 1.0, 2.5 M), and becomes weaker at higher concentrations (5 M). A possible reason could be that SPR is a more sensitive method than microscopy, taking into consideration the change of the effective refractive index on the substrate surface. The same observation was reported in a study of cell confluency during HeLa cell attachment and spreading (Deng et al., 2016), where the SPR results were much lower than cell confluency measured by microscopic imaging, although the overall trends were similar. They postulated it was because cells attached to the substrate with gaps in the cell-substrate contact, therefore the effective attachment area detected by SPR was less than the imaging attachment contour area. Nevertheless, our SPR results show very high correlations with cell confluency at lower H_2O_2 treatment concentrations (0.1 M–1.0 M), while the change of cell confluency was not as drastic as at higher concentrations.

Possible mechanisms behind the abnormal behavior at high concentration of H_2O_2

HeLa cells exposed to 5.0 M H_2O_2 exhibit different behavior between SPR signals and cell confluency measured with microscopic experimental method compared to the lower concentrations. Both SPR data and confluency data show a decreasing signal; however, after 5 min, the SPR signal keeps decreasing while the confluency signal first increases before then decreasing again at 30 min. Inspecting the microscopic image and calculated confluency, we can see HeLa cell confluency decreases in the first 5 min treatment with 5 M H_2O_2; next, the confluency increased and stabilized around 43% before decreasing to 37% (Figure 4B). This indicated that cell shrinkage occurred in the first 5 min before the cells underwent swelling, that increases confluency, before again reducing in size. This trend can be explained by the necrotic cell death mechanism. According to literature, necrosis is generally results at higher H_2O_2 treatment concentrations, whereas lower concentrations solely induce apoptosis (Rello et al., 2005; Troyano et al., 2003; McKeague et al., 2003). However, the time scale of treatment is an important factor as Troyano et al. (2003) found a portion of 0.2 mM H_2O_2 treated cells could be characterized as necrotic after a 14 h treatment. It has also been reported that a treatment with 0.1 M of H_2O_2 induced necrosis to HeLa cells first observable after 3 h (Rello et al., 2005). These results fit with the present study, where HeLa cell necrosis was observed rapidly with a 5.0 M H_2O_2 treatment but was not seen for lower concentrations within 2 h. Indicating the important interplay between concentration and treatment time to leads to apoptosis or necrosis.

As discussed previously, different morphological events occurred at high concentrations of H_2O_2 caused by simultaneous apoptosis and necrosis. Necrotic cells are distinguished from apoptotic cells by the amount of cell swelling, as observed after a 5-minute exposure time. We investigated this further by visually differentiating necrotic from apoptotic cells using microscopic images, and re-calculated percent confluency contributed by each condition. The results are shown in Figure 8, where we compared the total cell confluency (Figure 8B) with apoptotic (A) and necrotic (N) cell confluency (Figure 8C). We observed the cells were all necrotic

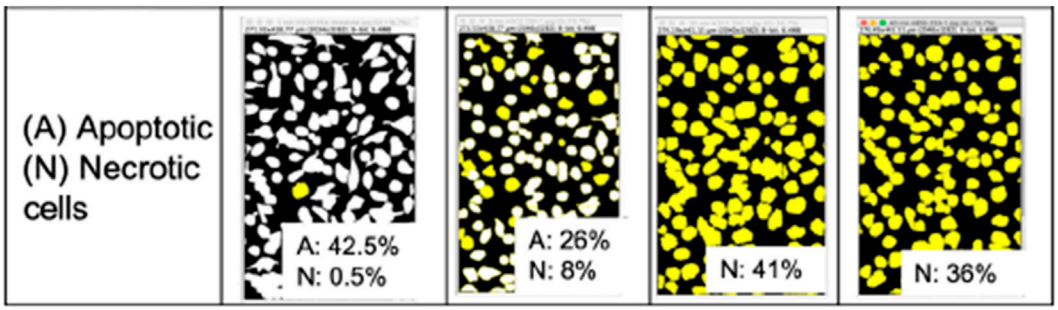

FIGURE 8
HeLa cell images after treatment with 5.0 M H_2O_2, separated based on apoptotic (white) and necrotic (yellow) cell contributions to total confluency. Analyzed from images shown in Figure 4.

after 20 min (41% confluency) and apoptotic blebs likely detached from the surface and floated into the solution, away from the surface, causing reduced confluency to 36% at 40 min.

In a study where HeLa cell morphological changes during apoptosis were observed using AFM (Kim et al., 2012), the images provided a better understanding of the size and thickness of the cells at the death stages, which support our observations. During the cell death progression as reported in the paper, the cells initially shrank, and then thickness increased. This explains why confluency decreases initially, before increasing, as the membranes start to become damaged followed by swelling. At this stage, the thickness keeps decreasing. As the blebs start detaching, the cells shrink again causing less confluency while the thickness increases. Evidently, there is a combination of size and thickness changes that were not able to be observed under the microscope but were detected by SPR due to the sensitivity of this method to minute changes on the surface. In addition, we found that the refractive index inside the cell body changes at different stages of apoptosis. This change itself is a result of changes to the intracellular biochemical components and volume (Zhang et al., 2017). Therefore, in addition to cell thickness, the intracellular refractive index is also a variable that changes during cell death that directly changes SPR response, as indicated in Equation 2. Furthermore, the derivation to achieve Equation 2 can be done in a more complex way for adlayer of cells, by factoring various cell shapes (Ramsden et al., 1994) in the formulation of the decay length, *ld*, instead of assuming the value to be 20%–50% of the wavelength of the light source.

It is a challenge to establish a comprehensive theoretical model associating all aspects of the SPR response to specific cell morphological changes. However, further development is important as SPR systems are clearly sensitive to these changes and could be used for real-time analysis of morphological changes. A few studies have addressed quantitative issues to study SPR response in cell-based applications (Ramsden et al., 1994; Deng et al., 2012; Fang et al., 2006). For example, a quantitative SPR was applied in a study of cell attachment, spreading, and proliferation phases by modifying the effective refractive index to include cell density and spreading area (Deng et al., 2016). However, the experimental SPR response agrees well with the calculated response only in the spreading phase, while the magnitude is largely different in the proliferation phase. Therefore, a revised mathematical model with a better fit between experimental and calculated SPR responses is still desired.

Conclusion

In conclusion, we have validated the potential of SPR spectroscopy to study morphological changes of HeLa cells induced by H_2O_2 by monitoring the changes in SPR signal in response to the change in cell confluency and cell detachment caused by cell death mechanisms. Several important findings were achieved. First, when compared with the microscopic images, we found that SPR signal decreases with decreasing cell confluency after the treatment with H_2O_2. Furthermore, the correlation was valid only at lower concentrations since 5.0 M concentration of H_2O_2 is not proportional to cell confluency because it induces apoptosis and necrosis simultaneously. Quantitative analysis of SPR signal in response to cell confluency was carried out to investigate other factors affecting the shift in SPR signal. The results verified the complexity of cell morphology that cannot be observed just by microscopy technique and that SPR is more sensitive to the changes on the cell-substrate interface. Although the mathematical model equation works in lower H_2O_2 concentrations, more complex derivations and simulations to solve complex mathematical models are needed. This is because cell activities change the morphology in many ways, including thickness of the cell layer, shapes, and the refractive index within the cell bodies. Therefore, for more accurate interpretation, the mathematical equation must include the aspects of non-uniform thicknesses, variable cell shapes, as well as changing refractive indexes of intracellular regions. Although SPR will not replace conventional cell-based assay to monitor cell responses to biological and chemical stimuli, or cell death inducers, it provides simple screening tools and quantifiable measurements comparable to other methods. This method can find broad applications for other living cells studies in medical fields, especially in drug development and clinical diagnosis.

Data availability statement

The raw data supporting the conclusions of this article will be made available by the authors, without undue reservation.

Ethics statement

Ethical approval was not required for the studies on humans in accordance with the local legislation and institutional requirements because only commercially available established cell lines were used.

Author contributions

NR: Conceptualization, Data curation, Formal Analysis, Investigation, Validation, Writing–original draft, Writing–review and editing. FA: Data curation, Formal Analysis, Investigation, Validation, Writing–original draft, Writing–review and editing. DS: Data curation, Formal Analysis, Validation, Writing–original draft, Writing–review and editing. WV: Data curation, Formal Analysis, Writing–original draft, Writing–review and editing. QC: Conceptualization, Data curation, Formal Analysis, Funding acquisition, Methodology, Supervision, Validation, Writing–original draft, Writing–review and editing.

Funding

The author(s) declare that financial support was received for the research, authorship, and/or publication of this article. We would like to acknowledge financial support from NSF (CHE-2109042).

Acknowledgments

The use of the University of California, Riverside nanofabrication facility to fabricate SPR chips/substrates used in this work is acknowledged.

Conflict of interest

The authors declare that the research was conducted in the absence of any commercial or financial relationships that could be construed as a potential conflict of interest.

The author(s) declared that they were an editorial board member of Frontiers, at the time of submission. This had no impact on the peer review process and the final decision.

Generative AI statement

The author(s) declare that no Generative AI was used in the creation of this manuscript.

Publisher's note

Supplementary material

The Supplementary Material for this article can be found online at: https://www.frontiersin.org/articles/10.3389/frans.2024.1518243/full#supplementary-material

References

Author Anonymous (2019). *PDQ® Adult Treatment Editorial Board. Cervical cancer treatment*. Bethesda, MD: National cancer institute. Available at: https://www.cancer.gov/types/cervical/hp/cervical-treatment-pdq

Bray, F., Ferlay, J., Soerjomataram, I., Siegel, R. L., Torre, L. A., and Jemal, A. (2018). Global cancer statistics 2018: GLOBOCAN estimates of incidence and mortality worldwide for 36 cancers in 185 countries. *CA Cancer J. Clin.* 68 (6), 394–424. doi:10.3322/caac.21492

Brown, W. E., and Wold, F. (1973). Alkyl isocyanates as active-site-specific reagents for serine proteases. Reaction properties. *Biochemistry* 12, 828–834. doi:10.1021/bi00729a007

Chabot, V., Cuerrier, C. M., Escher, E., Aimez, V., Grandbois, M., and Charette, P. G. (2009). Biosensing based on surface plasmon resonance and living cells. *Biosens. Bioelectron.* 24 (6), 1667–1673. doi:10.1016/j.bios.2008.08.025

Chen, K., Obinata, H., and Izumi, T. (2010). Detection of G protein-coupled receptor-mediated cellular response involved in cytoskeletal rearrangement using surface plasmon resonance. *Biosens. Bioelectron.* 25 (7), 1675–1680. doi:10.1016/j.bios.2009.12.006

Cooper, G. M. (2000). *The cell: a molecular approach*. Washington, D.C.: Sinauer Associates.

Deng, H., Wang, C., Su, M., and Fang, Y. (2012). Probing biochemical mechanisms of action of muscarinic M3 receptor antagonists with label-free whole cell assays. *Anal. Chem.* 84 (19), 8232–8239. doi:10.1021/ac301495n

Deng, S., Yu, X., and Wang, P. (2016). An irregular-shaped homogeneous refractive index model for interpretation of the surface plasmon resonance response from living cell attachment. *Anal. Methods* 8 (16), 3301–3306. doi:10.1039/c6ay00524a

Elmore, S. (2007). Apoptosis: a review of programmed cell death. *Toxicol. Pathol.* 35 (4), 495–516. doi:10.1080/01926230701320337

Fang, Y., Ferrie, A. M., Fontaine, N. H., Mauro, J., and Balakrishnan, J. (2006). Resonant waveguide grating biosensor for living cell sensing. *Biophys. J.* 91 (5), 1925–1940. doi:10.1529/biophysj.105.077818

Gomez Perez, M., Fourcade, L., Mateescu, M. A., and Paquin, J. (2017). Neutral Red versus MTT assay of cell viability in the presence of copper compounds. *Anal. Biochem.* 535, 43–46. doi:10.1016/j.ab.2017.07.027

Hemminki, K., and Granström, C. (2002). Morphological types of breast cancer in family members and multiple primary tumours: is morphology genetically determined? *Breast Cancer Res.* 4 (4), R7. doi:10.1186/bcr444

Hinman, S. S., Ruiz, C. J., Drakakaki, G., Wilkop, T. E., and Cheng, Q. (2015). On-demand formation of supported lipid membrane arrays by trehalose-assisted vesicle delivery for SPR imaging. *ACS Appl. Mater Interfaces* 7 (31), 17122–17130. doi:10.1021/acsami.5b03809

Joris, G., and Joris, I. (1995). Apoptosis, oncosis, and necrosis an overview of cell death. *JPJanuary* 146 (No 1), 3–15.

Kateryna, K., Sergiy, K., Leid, M., and Kioussi, C. (2012). Detection of apoptosis by TUNEL assay. *Methods Mol. Biol.* 887, 41–47. doi:10.1007/978-1-61779-860-3_5

Kim, K. S., Cho, C. H., Park, E. K., Jung, M. H., Yoon, K. S., and Park, H. K. (2012). AFM-detected apoptotic changes in morphology and biophysical property caused by paclitaxel in Ishikawa and HeLa cells. *PLoS One* 7 (1), e30066. doi:10.1371/journal.pone.0030066

Kumar, R., Srivastava, R., and Srivastava, S. (2015). Detection and classification of cancer from microscopic biopsy images using clinically significant and biologically interpretable features. *J. Med. Eng.* 2015, 457906. doi:10.1155/2015/457906

Linda, S., Jung, C. T. C., Chinowsky, T. M., Mar, M. N., and Yee, S. S. (1998). Quantitative interpretation of the response of surface plasmon resonance sensors to adsorbed films. *Langmuir* 14, 5636–5648. doi:10.1021/la971228b

Lowe, S. W., and Lin, A. W. (2000). Apoptosis in cancer carcinogenesis. *Carcinogenesis* 21 (3), 485–495. doi:10.1093/carcin/21.3.485

Maltais, J. S., Denault, J. B., Gendron, L., and Grandbois, M. (2012). Label-free monitoring of apoptosis by surface plasmon resonance detection of morphological changes. *Apoptosis* 17 (8), 916–925. doi:10.1007/s10495-012-0737-y

Marie-Veèronique, C., Shazib Pervaizc, A. P., and Pervaiz, S. (1998). Apoptosis induced by hydrogen peroxide is mediated by decreased superoxide anion concentration and reduction of intracellular milieu. *FEBS Lett.* 440, 13–18. doi:10.1016/s0014-5793(98)01410-0

McKeague, A. L., Wilson, D. J., and Nelson, J. (2003). Staurosporine-induced apoptosis and hydrogen peroxide-induced necrosis in two human breast cell lines. *Br. J. Cancer* 88 (1), 125–131. doi:10.1038/sj.bjc.6600675

Minet, O., Helfmann, J., Herrig, M., and Müller, G. (1996). The spatial variation of the refractive index in biological cells. *Phys. Med. Biol.* 41, 369–382. doi:10.1088/0031-9155/41/3/002

Moreira, B., Tuoriniemi, J., Kouchak Pour, N., Mihalcikova, L., and Safina, G. (2017). Surface plasmon resonance for measuring exocytosis from populations of PC12 cells: mechanisms of signal formation and assessment of analytical capabilities. *Anal. Chem.* 89 (5), 3069–3077. doi:10.1021/acs.analchem.6b04811

Rahmadwati, G. N., Ros, M., Todd, C., and Todd, C. (2012). "Morphological characteristics of cervical cells for cervical cancer diagnosis," in *Advances in intelligent and soft computing*. Editor J. Kacprzyk (Heidelberg New York Dordrecht London: Springer-Verlag Berlin Heidelberg), 2, 235–243. doi:10.1007/978-3-642-28308-6_32

Rajbongshi, N., Bora, K., Nath, D. C., Das, A. K., and Mahanta, L. B. (2018). Analysis of morphological features of benign and malignant breast cell extracted from FNAC microscopic image using the pearsonian system of curves. *J. Cytol.* 35 (2), 99–104. doi:10.4103/JOC.JOC_198_16

Ramsden, J. J., Prenosil, J. E., and Heinzle, E. (1994). Kinetics of adhesion and spreading of animal cells. *Biotechnol. Bioeng.* 43, 939–945. doi:10.1002/bit.260431007

Rello, S., Moreno, V., G´amez, A., Pacheco, M., Juarranz, A., Cañete, M., et al. (2005). Morphological criteria to distinguish cell death induced by apoptotic and necrotic treatments. *Apoptosis* 10, 201–208. doi:10.1007/s10495-005-6075-6

Robelek, R., and Wegener, J. (2010). Label-free and time-resolved measurements of cell volume changes by surface plasmon resonance (SPR) spectroscopy. *Biosens. Bioelectron.* 25 (5), 1221–1224. doi:10.1016/j.bios.2009.09.016

Schindelin, J., Arganda-Carreras, I., Frise, E., Kaynig, V., Longair, M., Pietzsch, T., et al. (2012). Fiji: an open-source platform for biological-image analysis. *Nat. Methods* 9 (7), 676–682. doi:10.1038/nmeth.2019

Singh, M., Sharma, H., and Singh, N. (2007). Hydrogen peroxide induces apoptosis in HeLa cells through mitochondrial pathway. *Mitochondrion* 7 (6), 367–373. doi:10.1016/j.mito.2007.07.003

Smith, S. M., Wunder, M. B., Norris, D. A., and Shellman, Y. G. (2011). A simple protocol for using a LDH-based cytotoxicity assay to assess the effects of death and growth inhibition at the same time. *PLoS One* 6 (11), e26908. doi:10.1371/journal.pone.0026908

Troyano, A., Sancho, P., Fernandez, C., de Blas, E., Bernardi, P., and Aller, P. (2003). The selection between apoptosis and necrosis is differentially regulated in hydrogen peroxide-treated and glutathione-depleted human promonocytic cells. *Cell Death Differ.* 10 (8), 889–898. doi:10.1038/sj.cdd.4401249

Yanase, Y., Hiragun, T., Ishii, K., Kawaguchi, T., Yanase, T., Kawai, M., et al. (2014). Surface plasmon resonance for cell-based clinical diagnosis. *Sensors (Basel)* 14 (3), 4948–4959. doi:10.3390/s140304948

Yanase, Y., Suzuki, H., Tsutsui, T., Hiragun, T., Kameyoshi, Y., and Hide, M. (2007). The SPR signal in living cells reflects changes other than the area of adhesion and the formation of cell constructions. *Biosens. Bioelectron.* 22 (6), 1081–1086. doi:10.1016/j.bios.2006.03.011

Zeiss, C. J. (2003). The apoptosis-necrosis continuum: insights from genetically altered mice. *Vet. Pathol.* 40, 481–495. doi:10.1354/vp.40-5-481

Zhang, Q., Zhong, L., Tang, P., Yuan, Y., Liu, S., Tian, J., et al. (2017). Quantitative refractive index distribution of single cell by combining phase-shifting interferometry and AFM imaging. *Sci. Rep.* 7 (1), 2532. doi:10.1038/s41598-017-02797-8